Increased El Niño amplitude during the last deglacial warming

Marco Yseki, Bruno Turcq, Dimitri Gutierrez, Renato Salvatteci, Dante Espinoza Morriberón, Hugues Boucher, Philippe Martinez, Matthieu Carré

Increased El Niño amplitude during the last deglacial warming

Marco Yseki (marco.yseki@gmail.com)
LOCEAN-IPSL Laboratory (UMR7159 CNRS-IRD-MNHN-Sorbonne Universit&#x0019;es)
https://orcid.org/0000-0002-8024-0615

Bruno Turcq
Center IRD France Nord, IRD Sorbonne University (UPMC, Univ. Paris 06) CNRS/MNHN, LOCEAN Laboratory, Bondy

Dimitri Gutierrez
Instituto del Mar del Perú (IMARPE)

Renato Salvatteci
Kiel University. Center for Ocean and Society

Dante Espinoza-Morriberón
Instituto del Mar del Perú

Hugues Boucher
LOCEAN-IPSL Laboratory (UMR7159 CNRS-IRD-MNHN-Sorbonne Universit&#x0019;es)

Philippe Martinez
EPOC

Matthieu Carré
LOCEAN-IPSL Laboratory (UMR7159 CNRS-IRD-MNHN-Sorbonne Universit&#x0019;es)

Article

Keywords:

Posted Date: February 17th, 2022

DOI: https://doi.org/10.21203/rs.3.rs-1303299/v1

Increased El Niño amplitude during the last deglacial warming

Marco Yseki[1*], Bruno Turcq[1], Dimitri Gutiérrez[2,3], Renato Salvatteci[4], Dante Espinoza-Morriberón[5,6], Hugues Boucher[1], Philippe Martinez[7] & Matthieu Carré[1,8]

1 LOCEAN-IPSL, Laboratoire d'Océanographie et du Climat: Expérimentation et Approches Numériques, Sorbonne Université/CNRS/IRD/MNHN, Paris, France.

2 Dirección General de Investigaciones Oceanográficas y de Cambio Climático, Instituto del Mar del Peru, Callao, Peru.

3 Laboratorio de Ciencias del Mar, Facultad de Ciencias y Filosofía, Universidad Peruana Cayetano Heredia, Lima, Peru.

4 Center for Ocean and Society, Kiel University, Kiel, Germany

5 Instituto del Mar del Peru, Laboratorio de Modelado Oceanográfico y de Cambio Climático, Callao, Peru.

6 Universidad Tecnológica del Peru (UTP), Facultad de Ingenieria, Lima, Peru.

7 UMR 5805 EPOC, Université de Bordeaux-CNRS-EPHE. Pessac Cedex, France.

8 Universidad Peruana Cayetano Heredia, Facultad de Ciencias y Filosofia, Centro de Investigación para el Desarrollo Integral y Sostenible, Laboratorios de Investigación y Desarrollo, Lima, Peru.

Abstract

It is still unclear how El Niño Southern Oscillation (ENSO), the leading mode of global-scale interannual climate variability, will respond to global warming. The last deglaciation offers natural experimental conditions to observe the behavior of ENSO in a period of abrupt warming and sea level rise. Here we present a record of ENSO-related interannual variability of river discharge in Peru during the last deglaciation (17.5-13 kyr BP) and the Late Holocene (2.7-1.4 kyr BP), based on high resolution records of Titanium in marine sediments from the Peruvian margin (Callao, 12ºS and Pisco 14ºS). We find that the amplitude of ENSO events was 50 to 190 % larger during the deglaciation compared to the Late Holocene, which supports the hypothesis that ENSO in the Eastern Pacific is strengthened by ice sheet meltwater discharge. A possible strengthening of ENSO in response to future ice sheet melting should be considered.

Introduction

The El Niño-Southern Oscillation (ENSO) is the main mode of interannual climate variability in the world[1,2] and especially affects South American precipitation through atmospheric teleconnections[3,4,5,6]. Large uncertainties in projections of ENSO reflect important gaps in our understanding of ENSO natural variability and its relationship with the mean climate state[7,8,9]. Reconstructions of ENSO centennial to millennial scale response to past natural climate change provide insights into the sensitivity of ENSO to changes in the background state and observational constraints to climate models[10,11].

The last deglaciation (~19-11 kyr BP) was a period of rapid global warming associated with a ~80 ppm increases in atmospheric CO_2[12]. The deglacial climate was also characterized by the melting of polar ice sheets[13] causing a rapid sea level rise[14] and a series of abrupt millennial-scale events[15]. The behavior of ENSO during the last deglaciation is still unclear. In the Eastern Equatorial Pacific (EEP), the spread of individual foraminifera Mg/Ca and $\delta^{18}O$ values estimated in three deglacial snapshots suggest a 16 to 60% increase in ENSO variability at 12.5, 15.1 and 17.9 kyr BP compared to the Late Holocene (1.6 kyr BP)[16], while no increase was found at 16.8 kyr BP using a different foraminifera species[17]. The lithic flux measured in the 106KL marine core from Callao, one of the few high-resolution records in the Eastern Tropical Pacific (ETP), was interpreted as a proxy for El Niño intensity[18]. However, the lithic flux has a fluvial and aeolian mixed origin in Callao[19], and the record's resolution for the last deglaciation did not allow to resolve the ENSO frequency band in this core.

In paleoclimate model experiments, deglacial meltwater pulses in the North Atlantic induce a weakening of the Atlantic Meridional Overturing Circulation (AMOC) intensity, a southern shift of the Intertropical Convergence Zone (ITCZ) and an increase in ENSO variability[20,21,22,23]. Meltwater forcing has been invoked to explain that ENSO in the early

Holocene was not as reduced as predicted by insolation forcing alone[24,25], but still requires to be tested with records from the deglaciation, when the meltwater flux was at its highest level. The last deglaciation is not equivalent to the current anthropogenic global warming, but offers us the opportunity to assess how ENSO characteristics were affected by this abrupt climate change.

Results and discussion

A high-resolution sediment record of ENSO variability

We present here a record of fluvial discharge interannual variability derived from high-resolution X-ray fluorescence Titanium (Ti-XRF) counts in two marine sediment cores collected on the Peruvian margin Peruvian margin (Fig. 1). The core M77/2-005-3 (12º05 S, 77º40,07 W) was collected off Callao at 214 m depth, and core G14 (14.38ºS, 76.42ºW) was collected off Pisco at 390 m depth. Despite sedimentation hiatus due to erosion, both cores record the last deglaciation (17.5-13 kyr BP) and a Late Holocene section (2.7-1.3 kyr BP) is recorded in Callao[19] (see depth-age models in supplementary Fig. 1). The sedimentation rate in the deglacial period, determined by 19 radiocarbon dates in Callao and 17 in Pisco is stable and high over the period (supplementary Fig. 1). The sections analyzed show irregularly spaced but well-preserved laminae indicating minimized sediment mixing (supplementary Fig. 2 and 3). The fast sedimentation (Late Holocene: 0.5 mm/yr in Callao; deglaciation: 1.2 mm/yr in Callao and 0.7 mm/yr in Pisco)[19] combined to the high resolution of the XRF measurements (1 mm) yields an unprecedented record of interannual climate variability in the ETP over thousands of years.

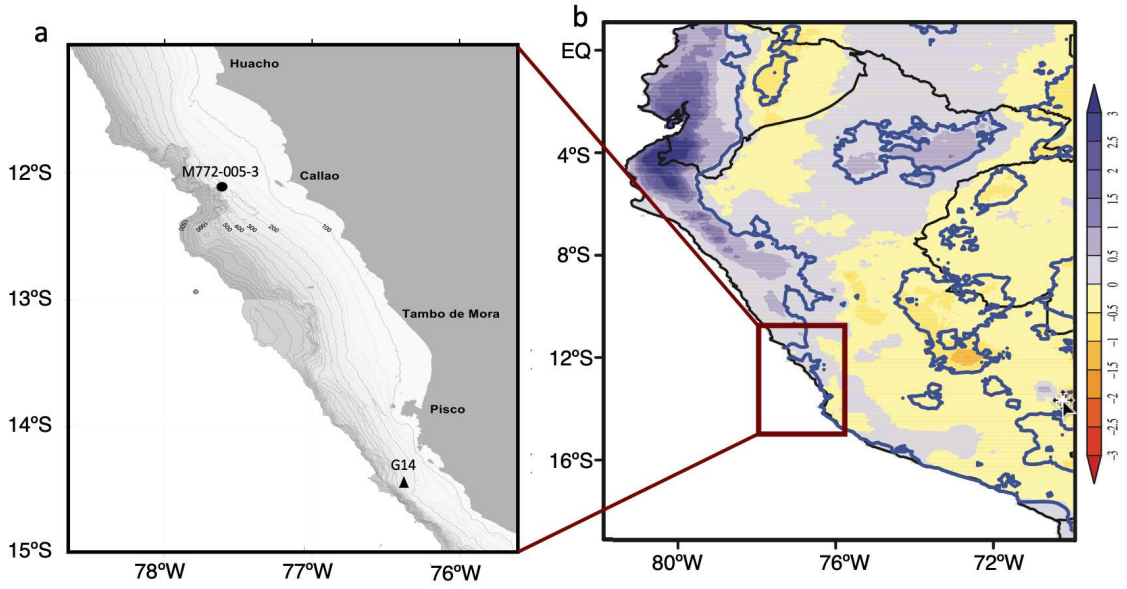

Figure 1. A) Location of the sampling of the sediment cores M77/2-005-3 (black circle) and G14 (black triangle) in the Peruvian margin. B) Linear regression coefficients between ENSO Eastern Pacific indices and precipitation (Figure adapted from Sulca *et al.*[5]).

Since Ti is relatively immobile during chemical weathering, Ti has been widely used as an indicator of terrigenous detrital input to sediments[26]. Ti-XRF variations in the central-southern Peruvian margin has been shown to be related to the fluvial fraction of terrestrial input[19] and is therefore used here as a proxy for river discharge (see Methods). The core M77/2-005-3 off Callao receives a Ti flux primarily from the discharge of the rivers Chancay, Chillón, Rimac, and Lurín, while the G14 core off Pisco is influenced by the Pisco and Ica rivers. Under the current climate, the flow of coastal rivers is usually low and increases during austral summer because of the monsoon rainfall in the High Andes[3,27,28]. During El Niño events, especially those with high sea surface temperature (SST) anomalies in the Eastern Pacific (EP), strong thunderstorms and precipitation occur on the coast[5,29,30,31,32]. These events produce catastrophic flash floods and large discharge of sediments during a few days[33,34,35].

Since Ti is related to river discharge and ENSO is the primary driver of interannual variability of rainfall in Peru, on the coast as well as in the Andes[5], the 2.5-8 year frequency band of Ti-XRF in Pisco and Callao sediment cores provide us with an unprecedented 4000-year long record of ENSO-related rainfall interannual variability during the last deglaciation. Ti-XRF counts records were normalized so that both cores could be compared (supplementary Fig. 4). Changes in the amplitude of interannual variability were estimated by the standard deviation of the 2.5-8 years band-pass filtered Ti-XRF series calculated over a 300-years long sliding window (see Methods).

Precipitation and ENSO in Peru during the deglaciation

Strong similarity is observed in the variations of Ti-XRF in Callao and Pisco during the last deglaciation, considering the chronological uncertainty (Fig. 2a). More importantly, the amplitude of Ti-XRF interannual variability varies coherently on millennial timescales in both sites (Fig. 2c). The regional scale reproducibility of the records demonstrates that the dataset is not affected by analytic or local biases and that Ti-XRF variations faithfully reflect regional scale climate variability.

Compared to the 1400-year long Late Holocene section, which can be considered as representative of modern conditions based on multiple studies[16,17, 24,25,36,37,38], higher Ti-XRF is found during the deglacial period (Fig. 2a). Lower sea level during the deglaciation might be partly responsible for the higher Ti-XRF off Callao and Pisco because of the reduced distance to the river mouths. However, the sediment source was only 20 km closer to the Callao core 18 kyr BP compared to today and at about the same distance for the Pisco core. In addition, the sea level rose strongly from 18 to 13 kyr BP, a trend that is not reflected in the Ti-XRF record, neither in Callao nor in Pisco. Hence, the larger deglacial Ti-XRF is likely the result of increased river discharge in central-

southern Peru. A deglacial increase in sediment discharge with a marked maximum during the Heinrich Stadial 1 cold spell was also recorded in a marine core from northern[38] and central-southern Peru[19]. Since coastal precipitation only occasionally occurs during strong El Niño events, the larger average river flow was likely primarily caused by increased precipitation in the Andes in agreement with records of strengthened south American monsoon in the central Andes[39,40,41,42] and evidence of a southern shift of the ITCZ mean position at that time[43,44,45].

We find a 50 to 190% increase in the amplitude of ENSO frequency band variability during the deglacial climate (17.5-13 kyr BP) compared to the Late Holocene (2.7-1.4 kyr BP) (Fig. 2c and 3g), when ENSO had similar to modern characteristics[11,17,24,25,46]. The record shows centennial to millennial scale modulation of ENSO amplitude is consistent with evidence obtained from individual foraminifera in the EEP[16] (Fig. 3f). ENSO amplitude is known to be subject to large decadal to centennial internal unforced variability [8,37,25,47] but is, during the deglaciation, consistently higher during more than 4000 years, compared to its modern level. The length of these interannual records (both of the Late Holocene and of the last deglaciation) yield an exceptional statistical robustness to this reconstruction of ENSO (for comparison, Holocene fossil corals and mollusks of the whole Pacific altogether record ~2500 years[25]). A robust increase of ENSO amplitude over such a long period could not be caused by stochastic internal variability. Therefore, the larger deglacial amplitude of ENSO must have been the result of a dynamical response to different boundary conditions.

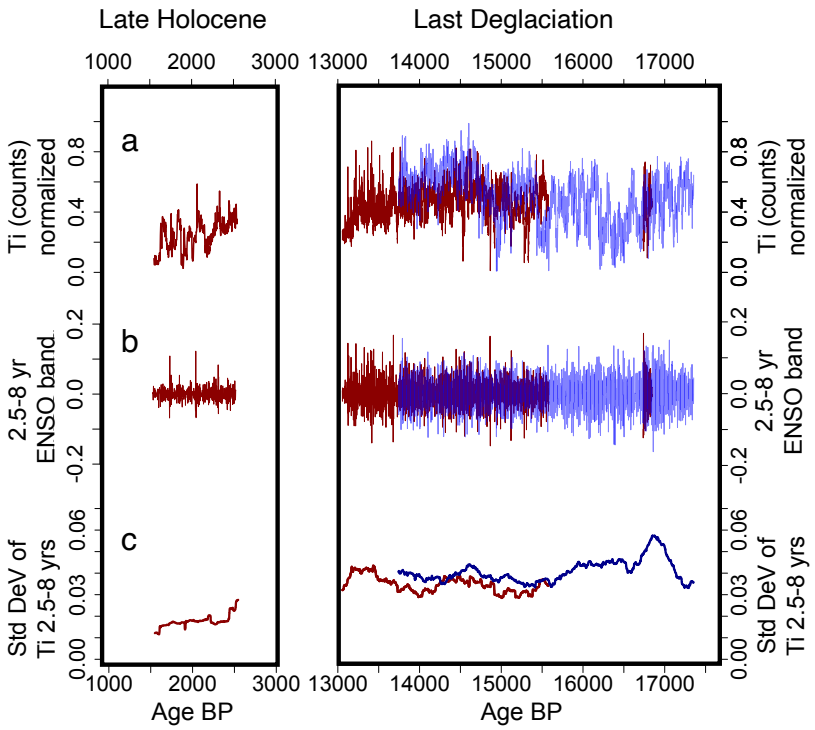

Figure 2. A) Ti-XRF counts normalized record in Callao (red) and Pisco (blue). B) 2.5-8 years frequency band of the Ti-XRF record in Callao (red) and Pisco (blue). C) Standard deviation (over 300 years moving windows) of the 2.5-8 years frequency band of the Ti-XRF record in Callao (red) and Pisco (blue) as a proxy of ENSO variability

ENSO and forcing mechanism during the last deglaciation

During the deglacial time, ENSO could have been affected by a number of forcing factors, including insolation, greenhouse gases, the presence of large polar ice sheets and meltwater discharge. The change in the seasonal flux of solar energy related to the Earth's orbital parameters has been shown to be a driver of ENSO in models [48,49,50] and to account for Holocene ENSO minimum (3-6 kyr BP) in paleoclimate records[25]. The damping effect of this external forcing was, however, stronger during the deglaciation and could therefore not explain the high variability recorded here (Fig 3a).

How increasing greenhouse gases influence ENSO is still unclear. While CMIP5 and CMIP6 models together tend to suggest an increased ENSO variability with increasing atmospheric CO_2 concentrations[51,52,53], two recent studies found that ENSO is weakening with increasing CO_2 when simulations last several millennia[8] or when model biases are

minimized with an ultra-high-resolution model[9]. The 80 ppm increase of CO_2 during the deglaciation is slightly lower than the current 100 ppm anthropogenic CO_2 increase that has not produced a clearly detectable impact on ENSO, and is much lower than the x2 or x4 scenarios tested for the future that yields contradictory effects. Thus, CO_2 changes could arguably be considered as a minor forcing of ENSO during the deglaciation.

In contrast to the Late Holocene, the deglaciation is mainly characterized by large remnant continental ice sheets and massive meltwater discharge[15,54,55,56,57]. The presence of a large ice sheet in the northern hemisphere strengthens the mid-latitude jet stream and remotely affects the tropical Pacific through atmospheric bridges and had a slight strengthening effect on ENSO in the EP in the IPSL-CM4 climate model[23]. Conversely, in the NCAR-CCSM3 transient simulation of the past 21,000 years forced uniquely by continental ice sheet variations, an abrupt ENSO increase (25%) is found at 14 kyr BP in response to a marked retreat of the Laurentide ice sheet[58]. This effect disappeared when all forcing were combined[58]. On the other hand, a meltwater discharge into the northern Atlantic consistently causes an increase of ENSO amplitude in multiple modeling experiments[20,21,22] and an eastward shift of anomalies[22,23,59], which would also result in increased variability in Peru. The 120 m sea level rise during the deglaciation[60] gives a measure of the magnitude of the corresponding meltwater flux into the North Atlantic and the Southern Ocean. Despite variations and some abrupt discharge events[61], the sea level never stopped rising from 20 to 7 kyr BP. The sustained meltwater flux during the whole deglaciation period seems thus the most likely forcing of the multi-millennial increase in ENSO strength recorded in Peru.

The AMOC is weakened by meltwater discharge in the North Atlantic and in the Southern Ocean[62,63,64]. The resulting change in the meridional-oceanic temperature gradient induces a southward displacement of the mean annual position of ITCZ, a weaker zonal

SST gradient across the equatorial Pacific and more symmetric annual mean climate in the EEP resulting in an amplified ENSO[20,21,22]. Although the underlying mechanisms responsible for the change in ENSO amplitude is still not clearly understood, the chain of response from the North Atlantic to the tropical Pacific is robust in model experiments.

Geochemical proxies of ocean circulation in marine sediments indicate a slowdown of the AMOC during the deglaciation due to large meltwater flux[65,66,67] (Fig. 3b). Records of tropical rainfall also point to a southern position of the mean annual position of the ITCZ in the deglaciation compared to the Late Holocene[43,44,45]. In addition, reduced zonal and meridional SST gradients were reconstructed in the Tropical Pacific (Fig. 3c) by Sadekov *et al*.[16] who also showed a strong link with ENSO amplitude. The deglacial climate, although rapidly changing, maintained an El Niño-like mean state in the tropical Pacific under the sustained influence of the meltwater flux weakening the AMOC. Our 4000-year long record shows that this mean state was associated with a long-term increase in El Niño amplitude in the EP, and provides observational support for the positive influence of meltwater flux on ENSO amplitude suggested by climate model experiments.

Very few model experiments have, however, explored the combined influence of multiple external forcing on ENSO during the deglaciation. The behavior of ENSO has been examined in the CCSM3 model TraCE-21ka transient simulation of the past 21 thousand years forced by orbital parameters, greenhouse gases, continental ice sheets and meltwater discharge, combined and separately[58]. Although meltwater discharge alone produces an increase in ENSO amplitude in the model, a compensation by the dampening effects of atmospheric CO_2 and insolation in TraCE-21ka results in a reduced ENSO during the last deglaciation[58] (Fig. 3e). Although TraCE-21ka reproduces correctly large-scale features of the evolution of the global climate (e.g., AMOC intensity, cross-Equator SST contrast, tropical Pacific SST)[58], the simulated deglacial reduction of ENSO is at odd

with the increased amplitude recorded in Peruvian sediments. This disagreement indicates an overestimation of the dampening effect of CO_2 and insolation and/or an underestimation of the response to meltwater discharge in this model, an issue that is possibly shared by other climate models.

An underestimation of the impact of meltwater discharge on the tropical climate variability in climate models raises serious issues in the context of current global warming. There is multiple evidence for a slowdown of AMOC in the 20th century, possibly as a result of Greenland ice sheet melting[68,69,70,71] which is accelerating with global warming[72]. The future weakening of AMOC was considered as very likely in IPCC AR5[73,74,75]. The impact of AMOC slowdown on ENSO has been so far overlooked in climate change projections, possibly because of uncertainties in icesheet melting rate, or undetected for an underestimated response in projections. However, our record of ENSO in the EP during the last great ice sheet melting period suggests that ENSO is more sensitive to freshwater flux than previously thought, pointing to a potential strengthening with future ice sheet melting in a greenhouse climate. Additional transient simulations of the last deglaciation are urgently needed to better assess the ability of models to predict ENSO response.

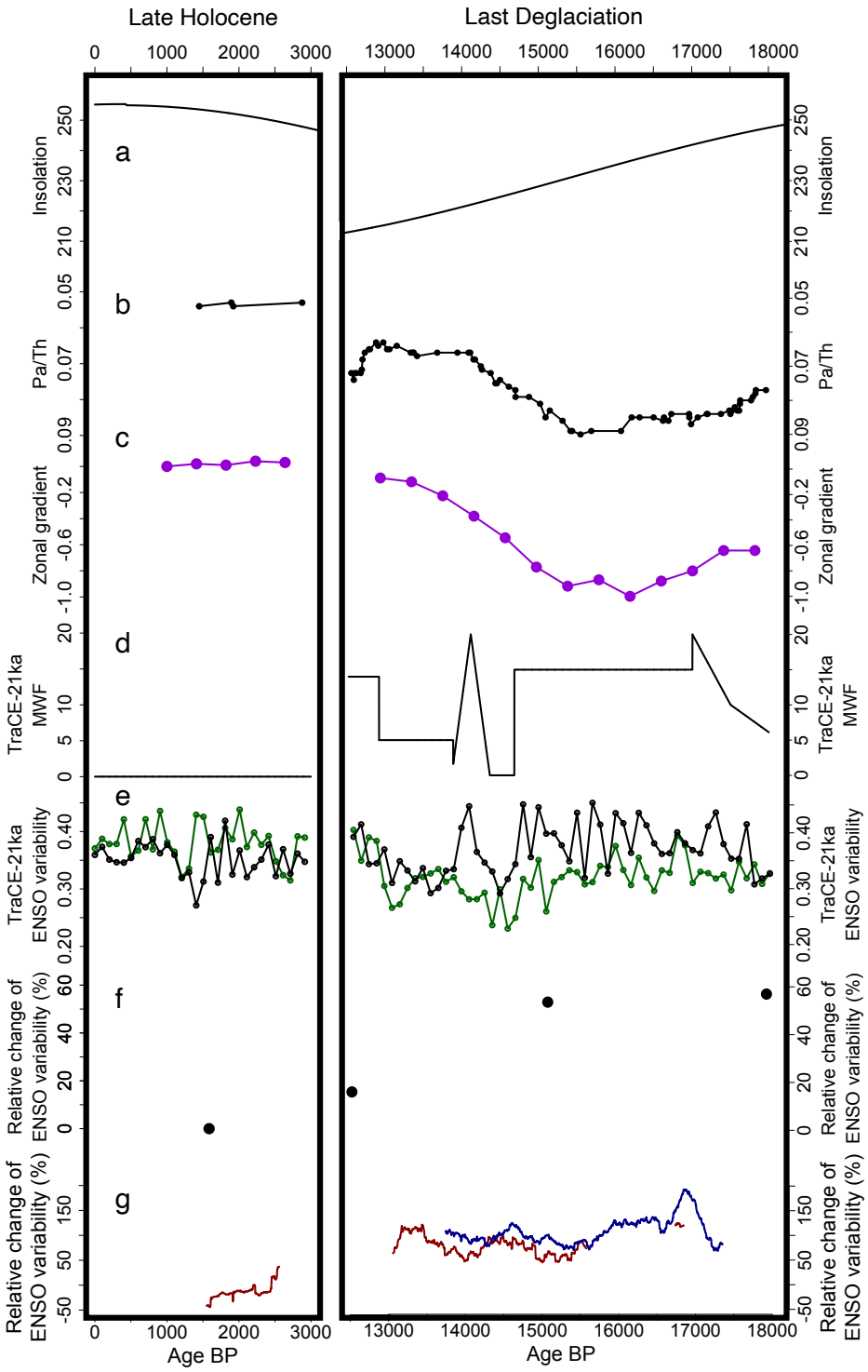

Figure 3. A) December, January and February minus June, July and August (DJF–JJA) insolation at 30ºS[76]. B) Composite $^{231}Pa/^{230}Th$ record that reflect past changes in AMOC[6]. C) Changes in zonal gradient across the equatorial Pacific[16]. D) Meltwater flux forcing (m/kyr) in TraCE-21ka[58]. E) ENSO variability in only meltwater flux experiment (black) and ENSO variability in all forcing experiment in TraCE-21ka (green)[58]. F) Individual foraminifera Mg/Ca variability[16]. G) ENSO-related interannual variability of river discharge in Callao (red) and Pisco (blue).

Methods

Marine sediments core

The cores M77/2-005-3 and G14 were retrieved from the Southeast Pacific continental slope during the M77-2 and Galathea-3 expedition respectively[77,78](Salvatteci et al., 2016, 2019). The lithology of both cores, previously described by Salvatteci *et al.*[77,78] is here complemented by X-Ray images and presented in supplementary Fig. 2 and 3. The Late Holocene and deglacial sediments are mainly composed of “irregularly spaced laminae” and “isolated laminae”, as defined by Brodie and Kemp[79]. The “irregularly spaced laminae” are packets of laminae (several centimeters to decimeters thick) separated by intervals of homogeneous sediments (several centimeters to decimeters thick). These laminae packages include alternations between diatom oozes and diatomaceous mud, the latter with a higher content of clay minerals. The "isolated laminae" are packets of millimetric and sub-millimetric laminae (solitary diatom ooze) enclosed in homogeneous mud. The G14 core is more finely laminated than the M77/2-005-3 core. Depth-age models based on 26 ^{14}C ages for the core M77/2-005-3 and 29 ^{14}C datings for G14 was built by Yseki *et al.*[19] and is presented for both cores in supplementary Fig. 1. The analyzed section (36-588 cm) of core M77/2-005-3 included the last deglaciation (17-13 kyr BP; 102-588 cm), and, above a sedimentation hiatus at 94 cm, part of the Late Holocene (2.7-1.4 kyr BP; 36-93 cm). Probably because of erosion, Holocene sediments were not recovered in G14. The analyzed section (10-285 cm) of core G14 included the last deglaciation (17.5-13.5 kyr BP)

XRF analysis

Ti was measured at high resolution (1 mm) in both cores using a XRF scanner only in the laminated or banded sections of the sediment cores in order to guarantee that the analyzed sections are a result of deposition from the water column and not from reworking of

upslope deposits[77]. XRF analysis were performed on core M77/2-005-3 and G14 at ALYSES facility (IRD-Sorbonne University, Bondy, France) and the University of Bordeaux 1 respectively. Measurements were done every 1 mm at 25kV and 500 uA during 10 s in core M772-005-3, and every 1 mm at 10kV and 400uA during 10 s in core G14.

Ti is present in marine sediments as titanium oxide resulting from soil pedogenesis and transported by rivers to the ocean along with clay minerals[80]. Ti-XRF has therefore been used as an indicator of river discharge, precipitation and ENSO variability[81,82]. XRF counts of Ti as well as other elements do not only depend on the mass concentration of Ti. It is also influenced by sediment heterogeneity that creates irregularities of the scanned core surface and mostly sediment inhomogeneity along the core such as variations in grain size or water content[83]. It is also influenced by the presence of elements that cannot be measured by this method, such as organic matter, causing a dilution effect, and more generally by matrix effects which includes the interactions of other elements present in the sediment on the XRF measurement of a given element[83]. For these reasons, the ratio or log ratio of XRF counts is frequently used in XRF core studies to correct for trends in sediment properties[38,84,85]. However, in the context of this study, which focuses on the high frequency variability of a sedimentary signal related to river inputs, considering the XRF counts of Ti in relation to another element would introduce an unnecessary noise that would disturb our analysis of the proxy fluctuation.

Centennial to millennial scale variations of fluvial and aeolian input during the last deglaciation were inferred from the grain size distribution in sediments from cores M77/2-005 and G14[19]. Downcore Ti-XRF variations in cores M77/2-005-3 and G14 covary with changes in fine particles of fluvial origin[19]. Maximum (minimum) Ti-XRF values occur when fluvial inputs increase (decrease) (supplementary Fig. 6), suggesting

that Ti-XRF is associated with particles of fluvial origin and not of aeolian and can be considered a potential proxy for fluvial discharges. To allow for the comparison of XRF data from different laboratories and different cores, a normalization to the maximum value of titanium counts was performed (supplementary Fig. 4).

Extracting ENSO amplitude

The XRF analyses with 1 mm steps yield a temporal resolution of 0.8 years in the deglacial sections of core M77/2-005-3, and 2.2 years in the Late Holocene section (2.7-1.3 kyr). The temporal resolution of the XRF record in the deglacial section of core G14 is 1.3 years.

The records were resampled by linear interpolation at 0.5-year resolution in the deglacial and Late Holocene sections (supplementary Fig. 5). A 2.5-8 years band pass filter was then applied to all records to extract the ENSO frequency band. The ENSO band was calculated based on the difference of moving averages. The amplitude of ENSO-related variability was estimated by the standard deviation of the filtered signal over 300-years moving windows. The relative change of ENSO variability in Callao and Pisco was calculated in reference to the Late Holocene record from Callao. The reproducibility of the normalized Ti-XRF records and of the filtered Ti-XRF standard deviation in Callao and Pisco allows us to use the Callao Late Holocene section as a common modern reference.

Acknowledgements

This publication was supported by the IRD-DPF and ANR-15-JCLI-0003-03 BELMONT FORUM PACMEDY. Part of XRF data were obtained on the ALYSES facility (IRD-UPMC) that was supported by grants from Région lIe-de-France. This work is a

contribution of the Collaborative Research Project 754 “Climate-Biogeochemistry interactions in the Tropical Ocean” (www.sfb754.de), which is supported by the Deutsche Forschungsgemeinschaft (DFG). We would like to thank the crew and scientists aboard R/V Meteor cruises M77/2 in 2008 and thank Bo Thamdrup, chief scientist of the Galathea-3 expedition (Leg 14), and Bente Lomstein, who conducted the core sampling onboard the RV Vaedderen.

Author contributions

MY, BT and MC designed the study. MY wrote the manuscript with greatest input of MC. RS, PM and HB measured XRF data. MY and DEM analyzed data. All authors contributed to the interpretation of the data and the preparation of the final manuscript.

References

1. Deser, C., Alexander, M., Xie, S. & Phillips, A. Sea Surface Temperature Variability: Patterns and Mechanisms. *Annual Review of Marine Science*2, 115-143 (2010).
2. McPhaden, M. J., Zebiak, S. E. & Glantz, M. H. ENSO as an Integrating Concept in Earth Science. *Science* **314,** 1740–1745 (2006).
3. Garreaud, R. D., Vuille, M., Compagnucci, R. & Marengo, J. Present-day South American climate. *Palaeogeography, Palaeoclimatology, Palaeoecology* **281,** 180–195 (2009).
4. Grimm, A. & Tedeschi, R. ENSO and Extreme Rainfall Events in South America. *Journal of Climate* 22, 1589-1609 (2009).
5. Sulca, J., Takahashi, K., Espinoza, J., Vuille, M. & Lavado-Casimiro, W. Impacts of different ENSO flavors and tropical Pacific convection variability (ITCZ, SPCZ) on austral summer rainfall in South America, with a focus on Peru. *International Journal of Climatology* 38, 420-435 (2017).
6. Cai, W. et al. Climate impacts of the El Niño–Southern Oscillation on South America. *Nature Reviews Earth & Environment* 1, 215-231 (2020).
7. Cai, W. et al. Changing El Niño–Southern Oscillation in a warming climate. *Nature Reviews Earth & Environment* 2, 628-644 (2021).
8. Callahan, C. et al. Robust decrease in El Niño/Southern Oscillation amplitude under long-term warming. *Nature Climate Change* 11, 752-757 (2021).
9. Wengel, C. et al. Future high-resolution El Niño/Southern Oscillation dynamics. *Nature Climate Change* 11, 758-765 (2021).
10. Braconnot, P. et al. Evaluation of climate models using palaeoclimatic data. *Nature Climate Change* 2, 417-424 (2012).

11. Emile-Geay, J. et al. Links between tropical Pacific seasonal, interannual and orbital variability during the Holocene. *Nature Geoscience* 9, 168-173 (2016).
12. Marcott, S. et al. Centennial-scale changes in the global carbon cycle during the last deglaciation. *Nature* 514, 616-619 (2014).
13. Peltier, W., Argus, D. & Drummond, R. Space geodesy constrains ice age terminal deglaciation: The global ICE-6G_C (VM5a) model. *Journal of Geophysical Research: Solid Earth* 120, 450-487 (2015).
14. Lambeck, K., Rouby, H., Purcell, A., Sun, Y. & Sambridge, M. Sea level and global ice volumes from the Last Glacial Maximum to the Holocene. *Proceedings of the National Academy of Sciences* 111, 15296-15303 (2014).
15. Clark, P. et al. Global climate evolution during the last deglaciation. *Proceedings of the National Academy of Sciences* 109, E1134-E1142 (2012).
16. Sadekov, A. et al. Palaeoclimate reconstructions reveal a strong link between El Niño-Southern Oscillation and Tropical Pacific mean state. *Nature Communications* 4, (2013).
17. Koutavas, A. & Joanides, S. El Niño-Southern Oscillation extrema in the Holocene and Last Glacial Maximum. *Paleoceanography* 27, (2012).
18. Rein, B. et al. El Niño variability off Peru during the last 20,000 years. *Paleoceanography* 20, n/a-n/a (2005).
19. Yseki, M. et al. Millennial variability of terrigenous transport to the central-southern Peruvian margin during the last deglaciation (18–13 kyr BP). Preprint at https://cp.copernicus.org/preprints/cp-2021-183/ (2022).
20. Timmermann, A. et al. The Influence of a Weakening of the Atlantic Meridional Overturning Circulation on ENSO. *Journal of Climate* 20, 4899-4919 (2007).
21. Merkel, U., Prange, M. & Schulz, M. ENSO variability and teleconnections during glacial climates. *Quaternary Science Reviews* 29, 86-100 (2010).
22. Braconnot, P., Luan, Y., Brewer, S. & Zheng, W. Impact of Earth's orbit and freshwater fluxes on Holocene climate mean seasonal cycle and ENSO characteristics. *Climate Dynamics* 38, 1081-1092 (2011).
23. Luan, Y., Braconnot, P., Yu, Y. & Zheng, W. Tropical Pacific mean state and ENSO changes: sensitivity to freshwater flux and remnant ice sheets at 9.5 ka BP. *Climate Dynamics* 44, 661-678 (2015).
24. Carré, M. et al. Holocene history of ENSO variance and asymmetry in the eastern tropical Pacific. *Science* 345, 1045-1048 (2014).
25. Carré, M. et al. High-resolution marine data and transient simulations support orbital forcing of ENSO amplitude since the mid-Holocene. *Quaternary Science Reviews* 268, 107125 (2021).
26. Haug, G., Hughen, K., Sigman, D., Peterson, L. & Röhl, U. Southward Migration of the Intertropical Convergence Zone Through the Holocene. *Science* 293, 1304-1308 (2001).
27. Vega-Jácome, F., Lavado-Casimiro, W. & Felipe-Obando, O. Assessing hydrological changes in a regulated river system over the last 90 years in Rimac Basin (Peru). *Theoretical and Applied Climatology* 132, 347-362 (2017).
28. Lavado Casimiro, W., Ronchail, J., Labat, D., Espinoza, J. & Guyot, J. Basin-scale analysis of rainfall and runoff in Peru (1969–2004): Pacific, Titicaca and Amazonas drainages. *Hydrological Sciences Journal* 57, 625-642 (2012).
29. Lagos, P., Silva, Y., Nickl, E. & Mosquera, K. El Niño – related precipitation variability in Perú. *Advances in Geosciences* 14, 231-237 (2008).
30. Lavado-Casimiro, W. & Espinoza, J. Impactos de El Niño y La Niña en las lluvias del Perú (1965-2007). *Revista Brasileira de Meteorologia* 29, 171-182 (2014).

31. Sanabria, J. et al. Rainfall along the coast of Peru during strong El Niño events. *International Journal of Climatology* 38, 1737-1747 (2017).
32. Bourrel, L. et al. Low-frequency modulation and trend of the relationship between ENSO and precipitation along the northern to centre Peruvian Pacific coast. *Hydrological Processes* 29, 1252-1266 (2014).
33. Morera, S., Condom, T., Crave, A., Steer, P. & Guyot, J. The impact of extreme El Niño events on modern sediment transport along the western Peruvian Andes (1968–2012). *Scientific Reports* 7, (2017).
34. Takahashi, K. & Martínez, A. The very strong coastal El Niño in 1925 in the far-eastern Pacific. *Climate Dynamics* 52, 7389-7415 (2017).
35. Guzman, E., Ramos, C. & Dastgheib, A. Influence of the El Niño Phenomenon on Shoreline Evolution. Case Study: Callao Bay, Perú. *Journal of Marine Science and Engineering* 8, 90 (2020).
36. Moy, C., Seltzer, G., Rodbell, D. & Anderson, D. Variability of El Niño/Southern Oscillation activity at millennial timescales during the Holocene epoch. *Nature* 420, 162-165 (2002).
37. Wittenberg, A. Are historical records sufficient to constrain ENSO simulations?. *Geophysical Research Letters* 36, (2009).
38. Mollier-Vogel, E., Leduc, G., Böschen, T., Martinez, P. & Schneider, R. Rainfall response to orbital and millennial forcing in northern Peru over the last 18 ka. *Quaternary Science Reviews* 76, 29-38 (2013).
39. Baker, P. et al. The History of South American Tropical Precipitation for the Past 25,000 Years. *Science* 291, 640-643 (2001).
40. Baker, P. et al. Tropical climate changes at millennial and orbital timescales on the Bolivian Altiplano. *Nature* 409, 698-701 (2001).
41. Martin, L. et al. Lake Tauca highstand (Heinrich Stadial 1a) driven by a southward shift of the Bolivian High. *Science Advances* 4, (2018).
42. González-Pinilla, F. et al. High- and low-latitude forcings drive Atacama Desert rainfall variations over the past 16,000 years. *Science Advances* 7, (2021).
43. Cheng, H., Sinha, A., Wang, X., Cruz, F. & Edwards, R. The Global Paleomonsoon as seen through speleothem records from Asia and the Americas. *Climate Dynamics* 39, 1045-1062 (2012).
44. Deplazes, G. et al. Links between tropical rainfall and North Atlantic climate during the last glacial period. *Nature Geoscience* 6, 213-217 (2013).
45. McGee, D., Donohoe, A., Marshall, J. & Ferreira, D. Changes in ITCZ location and cross-equatorial heat transport at the Last Glacial Maximum, Heinrich Stadial 1, and the mid-Holocene. *Earth and Planetary Science Letters* 390, 69-79 (2014).
46. Rodbell, D. et al. An ~15,000-Year Record of El Niño-Driven Alluviation in Southwestern Ecuador. *Science* 283, 516-520 (1999).
47. Cobb, K. M., Charles, C. D., Cheng, H. & Edwards, R. L. El Niño/Southern Oscillation and tropical Pacific climate during the last millennium. *Nature* **424,** 271–276 (2003).
48. Clement, A., Seager, R. & Cane, M. Orbital controls on the El Niño/Southern Oscillation and the tropical climate. *Paleoceanography* 14, 441-456 (1999).
49. Otto-Bliesner, B. El Niño/La Niña and Sahel precipitation during the Middle Holocene. *Geophysical Research Letters* 26, 87-90 (1999).
50. Brown, J. et al. Comparison of past and future simulations of ENSO in CMIP5/PMIP3 and CMIP6/PMIP4 models. *Climate of the Past* 16, 1777-1805 (2020).

51. Cai, W. et al. Increasing frequency of extreme El Niño events due to greenhouse warming. *Nature Climate Change* 4, 111-116 (2014).
52. Cai, W. et al. ENSO and greenhouse warming. *Nature Climate Change* 5, 849-859 (2015).
53. Cai, W. et al. Increased variability of eastern Pacific El Niño under greenhouse warming. *Nature* 564, 201-206 (2018).
54. Licciardi, J. M., Teller, J. T. & Clark, P. U. Freshwater routing by the Laurentide Ice Sheet during the last deglaciation. *Mechanisms of Global Climate Change at Millennial Time Scales* 177–201 (1999).
55. Carlson, A. & Clark, P. Ice sheet sources of sea level rise and freshwater discharge during the last deglaciation. *Reviews of Geophysics* 50, (2012).
56. Dynamics of meltwater discharge from Northern Hemisphere ice sheets during the last deglaciation. *Nature* 310, 674-677 (1984).
57. Brendryen, J., Haflidason, H., Yokoyama, Y., Haaga, K. & Hannisdal, B. Eurasian Ice Sheet collapse was a major source of Meltwater Pulse 1A 14,600 years ago. *Nature Geoscience* 13, 363-368 (2020).
58. Liu, Z. *et al.* Evolution and forcing mechanisms of El Niño over the past 21,000 years. *Nature* **515,** 550–553 (2014).
59. Williamson, M. et al. Effect of AMOC collapse on ENSO in a high resolution general circulation model. *Climate Dynamics* 50, 2537-2552 (2018).
60. Fairbanks, R. A 17,000-year glacio-eustatic sea level record: influence of glacial melting rates on the Younger Dryas event and deep-ocean circulation. *Nature* 342, 637-642 (1989).
61. Bard, E. et al. Deglacial sea-level record from Tahiti corals and the timing of global meltwater discharge. *Nature* 382, 241-244 (1996).
62. Seidov, D. Meltwater and the global ocean conveyor: northern versus southern connections. *Global and Planetary Change* 30, 257-270 (2001).
63. Stouffer, R., Seidov, D. & Haupt, B. Climate Response to External Sources of Freshwater: North Atlantic versus the Southern Ocean. *Journal of Climate* 20, 436-448 (2007).
64. Swingedouw, D., Fichefet, T., Goosse, H. & Loutre, M. Impact of transient freshwater releases in the Southern Ocean on the AMOC and climate. *Climate Dynamics* 33, 365-381 (2008).
65. McManus, J., Francois, R., Gherardi, J., Keigwin, L. & Brown-Leger, S. Collapse and rapid resumption of Atlantic meridional circulation linked to deglacial climate changes. *Nature* 428, 834-837 (2004).
66. Mulitza, S. et al. Synchronous and proportional deglacial changes in Atlantic meridional overturning and northeast Brazilian precipitation. *Paleoceanography* 32, 622-633 (2017).
67. Ng, H. et al. Coherent deglacial changes in western Atlantic Ocean circulation. *Nature Communications* 9, (2018).
68. Rahmstorf, S. et al. Exceptional twentieth-century slowdown in Atlantic Ocean overturning circulation. *Nature Climate Change* 5, 475-480 (2015).
69. Caesar, L., Rahmstorf, S., Robinson, A., Feulner, G. & Saba, V. Observed fingerprint of a weakening Atlantic Ocean overturning circulation. *Nature*556, 191-196 (2018).
70. Caesar, L., McCarthy, G., Thornalley, D., Cahill, N. & Rahmstorf, S. Current Atlantic Meridional Overturning Circulation weakest in last millennium. *Nature Geoscience* 14, 118-120 (2021).

71. Yang, Q. et al. Recent increases in Arctic freshwater flux affects Labrador Sea convection and Atlantic overturning circulation. *Nature Communications* 7, (2016).
72. Bevis, M. et al. Accelerating changes in ice mass within Greenland, and the ice sheet's sensitivity to atmospheric forcing. *Proceedings of the National Academy of Sciences* 116, 1934-1939 (2019).
73. Collins, M. et al. "Long-term climate change: projections, commitments and irreversibility." Climate Change 2013-The Physical Science Basis: Contribution of Working Group I to the Fifth Assessment Report of the Intergovernmental Panel on Climate Change. *Cambridge University Press*, 1029-1136 (2013).
74. Swingedouw, D. et al. On the reduced sensitivity of the Atlantic overturning to Greenland ice sheet melting in projections: a multi-model assessment. *Climate Dynamics* 44, 3261-3279 (2014).
75. Bakker, P. et al. Fate of the Atlantic Meridional Overturning Circulation: Strong decline under continued warming and Greenland melting. *Geophysical Research Letters* 43, 12,252-12,260 (2016).
76. Berger, A. Long-Term Variations of Daily Insolation and Quaternary Climatic Changes. *Journal of the Atmospheric Sciences* 35, 2362-2367 (1978).
77. Salvatteci, R. et al. Centennial to millennial-scale changes in oxygenation and productivity in the Eastern Tropical South Pacific during the last 25,000 years. *Quaternary Science Reviews* 131, 102-117 (2016).
78. Salvatteci, R., Schneider, R., Blanz, T. & Mollier-Vogel, E. Deglacial to Holocene Ocean Temperatures in the Humboldt Current System as Indicated by Alkenone Paleothermometry. *Geophysical Research Letters* 46, 281-292 (2019).
79. Brodie, I. & Kemp, A. Variation in biogenic and detrital fluxes and formation of laminae in late Quaternary sediments from the Peruvian coastal upwelling zone. *Marine Geology* 116, 385-398 (1994).
80. Yarincik, K., Murray, R. & Peterson, L. Climatically sensitive eolian and hemipelagic deposition in the Cariaco Basin, Venezuela, over the past 578,000 years: Results from Al/Ti and K/Al. *Paleoceanography* 15, 210-228 (2000).
81. Du, X. et al. Interannual Southern California Precipitation Variability During the Common Era and the ENSO Teleconnection. *Geophysical Research Letters* 47, (2020).
82. Du, X. et al. High-resolution interannual precipitation reconstruction of Southern California: Implications for Holocene ENSO evolution. *Earth and Planetary Science Letters* 554, 116670 (2021).
83. Weltje, G. & Tjallingii, R. Calibration of XRF core scanners for quantitative geochemical logging of sediment cores: Theory and application. *Earth and Planetary Science Letters* 274, 423-438 (2008).
84. Rothwell, R. & Rack, F. New techniques in sediment core analysis: an introduction. *Geological Society, London, Special Publications* 267, 1-29 (2006).
85. Perez, L., Crisci, C., Lüning, S., de Mahiques, M. & García-Rodríguez, F. Last millennium intensification of decadal and interannual river discharge cycles into the Southwestern Atlantic Ocean increases shelf productivity. *Global and Planetary Change* 196, 103367 (2021).

Supplementary Files

This is a list of supplementary files associated with this preprint. Click to download.

- Ysekietal2022ENSO.xlsx
- Ysekietal2022ENSOSI.pdf